

# THE CRUCIAL ROLE OF POROSITY ON DUST EVOLUTION IN PROTOPLANETARY DISKS

J.-F. Gonzalez<sup>1</sup> and S. Michoulier<sup>1</sup>

**Abstract.** In protoplanetary disks, millimeter- to centimeter-sized grains easily form from micrometric dust grains, but their further growth into planetesimals is hampered by several barriers, such as radial drift or fragmentation. The porosity of grains has been identified as a possible solution allowing to overcome these barriers. We present an improved model of the porosity evolution of dust aggregates as they grow, fragment, drift and settle, and apply it in numerical simulations of protoplanetary disks. We find that compaction during fragmentation is crucial to obtain sizes and porosities comparable to those observed in disks. Finally, we show that the evolution of porous grains can result in large areas in disks where the triggering conditions of the streaming instability, currently considered as the best mechanism to form planetesimals, are met.

Keywords: methods: numerical, planets and satellites: formation, protoplanetary disks

## 1 Introduction

Planets are formed in protoplanetary disks around young stars from the aggregation of sub-micrometer-sized dust grains. When they collide, they can stick thanks to van der Waals forces and reach mm- to cm-sized pebbles. At the other end of the mass spectrum, where self-gravity becomes important, kilometer-sized planetesimals can grow into planets. The main bottleneck lies in the intermediate range because of so-called barriers to planet formation, such as radial drift or fragmentation, which hinder the growth of pebbles into planetesimals.

Proposed solutions invoke a thin and dense layer of pebbles where concentration mechanisms such as self-induced dust traps (Gonzalez et al. 2017; Vericel & Gonzalez 2020) or instabilities can facilitate solid growth past these barriers. The streaming instability (SI, Youdin & Goodman 2005) is currently thought to be the best mechanism able to form planetesimals. It can lead to strong particle clumping if the following conditions are met in the disk midplane: a Stokes number (ratio of the drag stopping time to the orbital time)  $St \sim 0.01-1$ , a dust-to-gas mass ratio  $\varepsilon \gtrsim 0.3-0.5$  and a dimensionless pressure gradient  $\Pi = \Delta v/c_s > 0.01$ , where  $\Delta v$  is the differential velocity between gas and dust and  $c_s$  the gas sound speed (Li & Youdin 2021). However, whether these triggering criteria are met in real disks has not yet been verified.

Grain porosity has also been proposed as a solution: compared to compact grains of the same mass, they have a larger cross-section, collide with more neighboring grains, and grow faster. They reach the Stokes drag regime sooner, in which they decouple faster from the gas as they grow, and can escape the radial-drift barrier (Okuzumi et al. 2012; Garcia & Gonzalez 2020).

We present here an improved porosity evolution model, assess how it affects the grain population in disks, and examine its impact on the SI triggering criteria.

## 2 Methods

### 2.1 Porosity evolution model

To model porosity, we consider grains as spheres of radius  $s$  containing identical compact monomers, also spherical, and void between them. A grain's filling factor  $\phi$  is defined as the fraction of its volume that is occupied by matter. It is also the ratio of the average grain density to the density of the monomers. When two

---

<sup>1</sup> Université Claude Bernard Lyon 1, CRAL UMR5574, ENS de Lyon, CNRS, Villeurbanne, F-69622, France

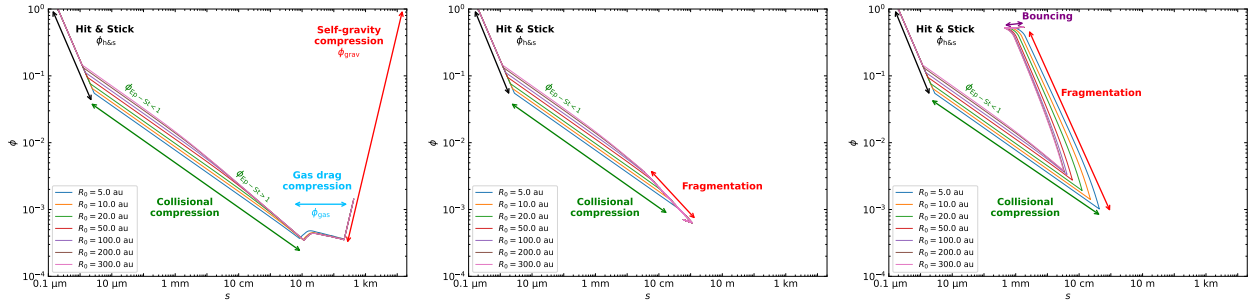


**Fig. 1.** Porosity evolution model: filling factor  $\phi$  as a function of size  $s$  for different initial distances to the star  $R_0$  for silicate grains composed of  $0.2 \mu\text{m}$  monomers in our standard disk model. **Left:** Growth only. **Center:** Growth and fragmentation. **Right:** Growth, fragmentation with compaction, and bouncing.

grains collide and stick, they form a larger grain, enclosing an additional volume of void (Okuzumi et al. 2012). Grains thus become more porous as they grow. This is illustrated in the ‘hit and stick’ regime in the left panel of Fig. 1, showing  $\phi$  as a function of  $s$  for grains of various initial location in a protoplanetary disk. Grains start as compact ( $\phi = 1$ ) monomers of size  $s = 0.2 \mu\text{m}$ , in the top left corner. As they grow, they move to the right of the plot, and become more porous, moving downwards. They then enter the collisional compression regime, where excess collisional kinetic energy is used to compact them. They still become more porous, but more slowly: their trajectory in the  $(s, \phi)$  plane becomes shallower. For even larger grains, gas drag becomes efficient at compressing them further. Finally, for bodies of a few hundred meters, self-gravity becomes important and compresses them back to compact bodies, tens of km in size.

However, grains do not grow unhindered: they meet the fragmentation barrier when their relative velocity during collisions exceeds the threshold  $v_{\text{frag}}$ , and they no longer grow but shatter into small grains. Assuming that their porosity stays constant during fragmentation, their trajectory in the  $(s, \phi)$  is limited to cm sizes, with filling factors of a few  $10^{-3}$ , as shown in the central panel of Fig. 1. When grains are allowed to be compacted in destructive collisions,  $\phi$  increases when  $s$  decreases (right panel of Fig. 1). Finally, when they reach  $\phi \sim 0.3$ , bouncing starts to be important and compacts them only slightly more.

Full details on the porosity evolution model and how to compute  $\phi$  in different regimes of grain growth and fragmentation can be found in Michoulier et al. (2024a).

## 2.2 Numerical simulations

We used the 3D Smoothed Particle Hydrodynamics (SPH) code PHANTOM (Price et al. 2018) to compute the evolution of a protoplanetary disk composed of gas and silicate dust grains, orbiting a  $1 M_{\odot}$  star. The gas disk has a mass  $M_{\text{disk}} = 0.01 M_{\odot}$  and is set up with a surface density profile  $\Sigma \propto (r/r_0)^{-0.75}$  extending from  $R_{\text{in}} = 10 \text{ au}$  to  $R_{\text{out}} = 400 \text{ au}$ . Its temperature profile  $T \propto (r/r_0)^{-0.5}$  is set by the choice of the aspect ratio  $(H/R)_0 = 0.0895$  at  $r_0 = 100 \text{ au}$ . The dust grains are initially distributed with a uniform dust-to-gas mass ratio of  $\varepsilon_0 = 0.01$ . We used the ‘dust-as-mixture’ formalism with 1.2 million SPH particles and a turbulent viscosity parameter (Shakura & Sunyaev 1973)  $\alpha = 5 \times 10^{-3}$ . Our silicate grains have an intrinsic density  $\rho_s = 2700 \text{ kg m}^{-3}$  and a fragmentation threshold  $v_{\text{frag}} = 20 \text{ m s}^{-1}$ . The CO snow line is modeled by a jump in  $v_{\text{frag}}$  down to  $5 \text{ m s}^{-1}$  where  $T < 20 \text{ K}$  ( $r \gtrsim 100 \text{ au}$  in our disk). We evolved the simulations for 300 000 yr. More information on the simulation suite and setup is given in Michoulier et al. (2024a).

## 3 Results

We consider four simulations: the first one contains compact grains that grow and fragment, the second one allows grains to be porous, the third one adds compaction during fragmentation, and the fourth one includes the CNO snowline. Figure 2 shows snapshots of these four simulations (from left to right) at  $t = 100\,000 \text{ yr}$ , displaying the grain size in the meridian plane (top) and the radial grain size distribution, colored by filling factor (bottom). Settling is efficient and comparable in all cases interior to  $\sim 100 \text{ au}$ . In the outer disk, porous grains smaller than the millimeter are still well coupled to the gas and have settled very little. As expected (see Sect. 1), porous grains grow more efficiently and reach centimeter sizes, while they become very fluffy, with

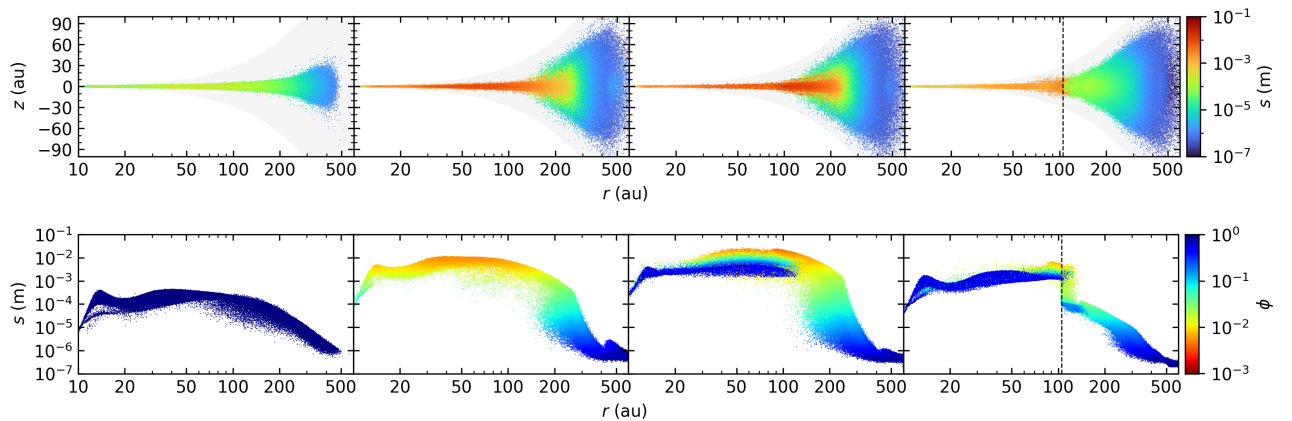


**Fig. 2.** Snapshot at  $t = 100\,000$  yr of the evolution of silicate grains with growth and fragmentation. **Top:** Grain size  $s$  in the meridian plane  $(r, z)$ , with the light gray background showing the gas disk. **Bottom:** Radial grain size distribution, with color representing the filling factor  $\phi$ . **From left to right:** Compact grains, porous grains, porous grains with compaction, porous grains with compaction and the CO snow line (marked by the vertical dotted line).

filling factors as low as a few  $10^{-3}$ , whereas compact grains only grow up to a few hundred micrometers. When compaction is included, porous grains are compressed back to sizes of a few millimeters and filling factors of a few tenths. We chose the  $t = 100\,000$  yr snapshot because it best shows the grains being compacted from  $\phi \sim 2 \times 10^{-3}$  to  $\sim 0.3$ . After  $200\,000$  yr, all grains interior to  $200$  au are compacted (not shown). Outside of the CO snow line, grains are more fragile due to their CO-ice coating and grow much more slowly, remaining smaller than  $100\ \mu\text{m}$ .

In the midplanes of observed protoplanetary disks, grains are generally found to larger than  $0.3\text{--}1$  mm, with filling factors  $\phi \sim 0.1\text{--}1$  (e.g. Zhang et al. 2023; Ohashi et al. 2023). In our simulations, compact grains are too small, and porous grains too fluffy to reproduce observations. It’s only when compaction is included that both sizes and porosities are compatible with observations. When the CO snow line is taken account, this is the case interior to it.

We now consider the last two (realistic) cases to examine if and where the triggering criteria of the SI are met. Figure 3 shows maps of  $\varepsilon$  (top),  $St$  (middle), and  $\Pi$  (bottom) in the meridian plane of our modeled disk for porous grains including compaction, without (left) and with (right) the CO snow line. The highlighted regions in the top panel mark the locations in the disk where  $\varepsilon \geq 0.5$ , and the  $St$  and  $\Pi$  maps are shown only within those regions in the bottom two panels, where the range of values explored by these parameters are shown in their top left corner.

In the simulation without CO snow line (left),  $\varepsilon \geq 0.5$  in only two small disk regions, where the criteria for  $St$  and, to a lesser extent,  $\Pi$  (the outer part of the inner region has  $\Pi < 0.01$ ) are also met. The SI can thus lead to particle clumping, but only in very limited parts of the disk. This can be an issue as noted by Carrera & Simon (2022), because drifting grains can cross them faster than the SI can grow. At later times (not shown), these regions grow, but still cover only a fraction of the disk.

The simulation taking the CO snow line into account (right) results in all three criteria being met in most of the disk interior to  $100$  au, and not limited to the midplane. The conditions for particles to clump and ultimately be able to form planetesimals are thus very favorable when all the realistic processes (grain porosity, growth, fragmentation with compaction, bouncing, and the CO snow line) are included.

## 4 Conclusion

We ran simulations of the evolution of compact and porous silicates grains in a typical protoplanetary disk and compared the resulting sizes and porosities to those measured in observed disks. We found that compact grains remain too small, it is thus necessary to take grain porosity into account. Similarly, compaction during fragmentation is needed because without it, grains become too porous. Finally, the CO snow line helps to retain more grains in the disk and produces larger regions where the SI triggering conditions are met, thus facilitating planetesimal formation.

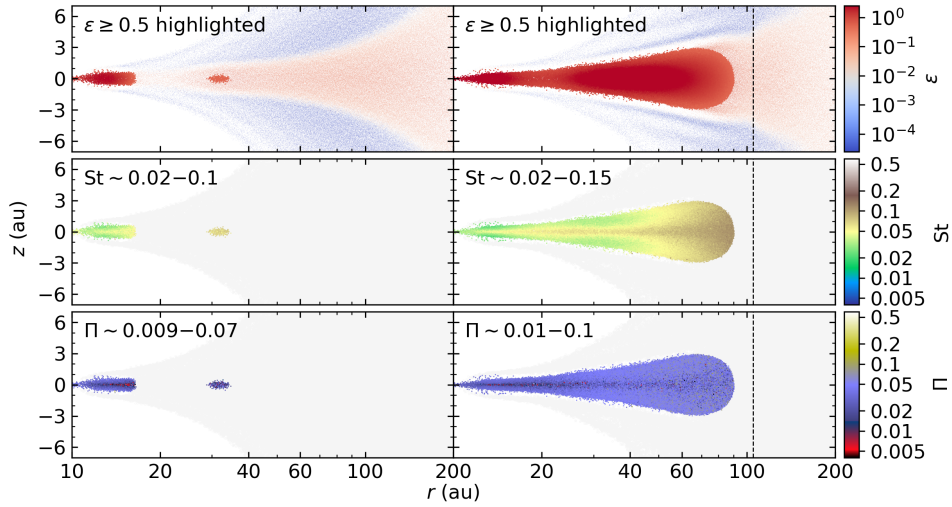


**Fig. 3.** Maps of the dust-to-gas ratio  $\varepsilon$  (**top**), the Stokes number  $St$  (**middle**), and the dimensionless pressure gradient  $\Pi$  (**bottom**) in the meridian plane for silicate grains with growth, fragmentation and compaction, without (**left**) and with (**right**) the CO snow line (marked by the vertical dotted line) at  $t = 150\,000$  yr. In the top row, the darker regions highlight where  $\varepsilon \geq 0.5$ . In the bottom two rows, maps of  $St$  and  $\Pi$  are only shown within those regions. Outside of them, the light gray color shows the gas disk.

The authors acknowledge funding from ANR (Agence Nationale de la Recherche) of France under contract number ANR-16-CE31-0013 (Planet-Forming-Disks) and thank the LABEX Lyon Institute of Origins (ANR-10-LABX-0066) for its financial support within the Plan France 2030 of the French government operated by the ANR. This research was partially supported by the Programme National de Physique Stellaire and the Programme National de Planétologie of CNRS (Centre National de la Recherche Scientifique)/INSU (Institut National des Sciences de l’Univers), France. We gratefully acknowledge support from the PSMN (Pôle Scientifique de Modélisation Numérique) of the ENS de Lyon for the computing resources. This project has received funding from the European Union’s Horizon 2020 research and innovation programme under the Marie Skłodowska-Curie grant agreements No 210021 and No 823823 (DUSTBUSTERS). Figures were made with the Python library matplotlib (Hunter, 2007). The data necessary to recreate the PHANTOM simulations and to reproduce the corresponding figures are available in Michoulier et al. (2024b).

## References

- Carrera, D. & Simon, J. B. 2022, *ApJ*, 933, L10  
 Garcia, A. J. L. & Gonzalez, J.-F. 2020, *MNRAS*, 493, 1788  
 Gonzalez, J. F., Laibe, G., & Maddison, S. T. 2017, *MNRAS*, 467, 1984  
 Hunter, J. D. 2007, *Computing in Science & Engineering*, 9, 90  
 Li, R. & Youdin, A. N. 2021, *ApJ*, 919, 107  
 Michoulier, S., Gonzalez, J.-F., & Price, D. J. 2024a, *A&A*, 688, A31  
 Michoulier, S., Gonzalez, J.-F., & Price, D. J. 2024b, Dumps and Data for ‘Compaction during fragmentation and bouncing produces realistic dust grain porosities in protoplanetary discs’, dataset, Zenodo, <https://doi.org/10.5281/zenodo.12729015>  
 Ohashi, S., Momose, M., Kataoka, A., et al. 2023, *ApJ*, 954, 110  
 Okuzumi, S., Tanaka, H., Kobayashi, H., & Wada, K. 2012, *ApJ*, 752, 106  
 Price, D. J., Wurster, J., Tricco, T. S., et al. 2018, *PASA*, 35, e031  
 Shakura, N. I. & Sunyaev, R. A. 1973, *A&A*, 24, 337  
 Vericel, A. & Gonzalez, J.-F. 2020, *MNRAS*, 492, 210  
 Youdin, A. N. & Goodman, J. 2005, *ApJ*, 620, 459  
 Zhang, S., Zhu, Z., Ueda, T., et al. 2023, *ApJ*, 953, 96